—— **Review** ——

Techniques for predicting the lifetimes of wave-swept macroalgae: a primer on fracture mechanics and crack growth

Katharine J. Mach[1,*], Drew V. Nelson[2] and Mark W. Denny[1]

[1]*Hopkins Marine Station of Stanford University, Pacific Grove, CA 93950, USA and* [2]*Department of Mechanical Engineering, Stanford University, Stanford, CA 94305, USA*

*Author for correspondence (e-mail: mach@stanford.edu)

Summary

Biomechanical analyses of intertidal and shallow subtidal seaweeds have elucidated ways in which these organisms avoid breakage in the presence of exceptional hydrodynamic forces imposed by pounding surf. However, comparison of algal material properties to maximum hydrodynamic forces predicts lower rates of breakage and dislodgment than are actually observed. Why the disparity between prediction and reality? Most previous research has measured algal material properties during a single application of force, equivalent to a single wave rushing past an alga. In contrast, intertidal macroalgae may experience more than 8000 waves a day. This repeated loading can cause cracks – introduced, for example, by herbivory or abrasion – to grow and eventually cause breakage, yet fatigue crack growth has not previously been taken into account. Here, we present methods from the engineering field of fracture mechanics that can be used to assess consequences of repeated force imposition for seaweeds. These techniques allow quantification of crack growth in wave-swept macroalgae, a first step towards considering macroalgal breakage in the realistic context of repeated force imposition. These analyses can also be applied to many other soft materials.

Key words: fracture mechanics, breakage, fatigue, intertidal, macroalgae, seaweed, biomechanics.

Introduction

Wave-swept rocky shores are one of the most physically severe habitats on the planet. At low tide, organisms in the intertidal zone are exposed to terrestrial rigors, including substantial temperature fluctuations, desiccation and increased insolation (Denny and Wethey, 2001; Tomanek and Helmuth, 2002). At high tide, breaking waves are accompanied by water velocities that often exceed $10\ \mathrm{m\,s^{-1}}$ and impose large hydrodynamic forces (e.g. Dudgeon and Johnson, 1992; Gaylord, 1999; Gaylord, 2000; Denny and Gaylord, 2002; Denny, 2006). Nonetheless, communities of organisms in this harsh environment are highly diverse and productive (Smith and Kinsey, 1976; Connell, 1978; Leigh et al., 1987). The unusual presence of dense and diverse assemblages of organisms in a stressful environment, coupled with the experimental tractability of the system (as a result of steep environmental gradients, rapid turnover of organisms, and abundant sessile and slow-moving organisms), has made wave-swept shores a test bed for ecomechanics. The connections between community ecology (e.g. Paine, 1966; Paine, 1984; Dayton, 1971; Connell, 1978; Menge, 1995; Bertness and Leonard, 1997; Harley and Helmuth, 2003), physiology (e.g.

Wolcott, 1973; Hofmann and Somero, 1995; Stillman and Somero, 1996; Somero, 2002; Stillman, 2002; Tomanek, 2002) and physical adaptations (e.g. Koehl, 1986; Carrington, 1990; Blanchette, 1997; Martone, 2006) of intertidal and nearshore organisms have been explored for decades.

Even though physical and physiological intertidal stresses are repetitive in nature, associated with the flow and ebb of tides, most experiments have focused on acute lethal stresses and repercussions for competitive ecological interactions. Sublethal consequences of repeated desiccation, high and low temperatures, hydrodynamic forces and other environmental conditions have proven difficult to address (e.g. Koehl, 1984; Koehl, 1986; Davison and Pearson, 1996). Here we describe methods for quantifying the potentially lethal effects of repeated hydrodynamic forces.

Hydrodynamic consequences for macroalgae

Although intertidal seaweeds occur in myriad forms, their morphologies share some common elements. A macroalga attaches to the substratum *via* a holdfast, from which one or several stem-like structures (often called stipes) emerge. Each

stipe supports one or more blades. Together holdfast, stipe(s), and blade(s) constitute the thallus of the alga.

For seaweeds, hydrodynamic stresses imposed on thalli represent a substantial facet of rocky shores' extreme physical environment. Subtidally, water velocities reach several m s^{-1} (Denny, 1988), while magnitudes of water velocities increase manyfold intertidally (commonly to 10–20 m s^{-1}) as waves break and are funneled by substratum topography (Denny et al., 2003; Denny, 2006).

Intertidal macroalgae, as sessile organisms, cannot actively avoid the violent water motion of the wave-swept environment. Instead, as water flows past an intertidal seaweed, the water exerts force, primarily drag, on the organism (Gaylord et al., 1994; Gaylord, 2000; Boller and Carrington, 2006a). Intertidal macroalgae thus experience forces, predominantly in tension, throughout their lengths with each passing wave. And macroalgae endure substantial forces: drag forces imposed by water moving at 10 m s^{-1} are comparable to the forces that would be exerted by winds traveling at 1050 km h^{-1}, nearly Mach 1, if air were incompressible. Furthermore, intertidal seaweeds must endure these hydrodynamic forces frequently; approximately 8600 waves break on shore each day.

Many biomechanical studies have investigated the mechanical properties and morphological attributes that enable wave-swept macroalgae to survive drag forces imposed by breaking waves (e.g. Carrington, 1990; Holbrook et al., 1991; Denny and Gaylord, 2002; Pratt and Johnson, 2002; Kitzes and Denny, 2005; Martone, 2006). These studies have investigated algal material properties primarily in tensile tests, finding macroalgae highly extensible and generally compliant (the opposite of stiff), with low breaking strength, compared to other biomaterials (Hale, 2001; Denny and Gaylord, 2002). In addition, investigations have suggested the importance of algal flexibility, which is in part a consequence of the compliance of algal materials. Seaweeds align, deform and bundle with flow, thereby reconfiguring to reduce drag (Vogel, 1984; Koehl, 1986; Boller and Carrington, 2006b).

To date, studies of algal materials have evaluated their abilities to resist large wave forces through pull-to-break tests, in which samples are loaded in tension until they break. The force required for breakage, normalized as stress (applied bulk force per initial material cross-sectional area), is taken as the ultimate strength, or breaking stress, of the material. This strength is then compared to the stresses imposed by the largest waves to predict an alga's risk of breakage. These comparisons have repeatedly predicted low probabilities of breakage (e.g. Koehl and Alberte, 1988; Gaylord et al., 1994; Gaylord, 2000; Johnson and Koehl, 1994; Friedland and Denny, 1995; Utter and Denny, 1996; Denny et al., 1997; Johnson, 2001; Kitzes and Denny, 2005), leading to the suggestion that wave-swept algae are mechanically over-designed (Denny, 2006).

However, these predictions are at odds with reality: many seaweeds experience consistent, substantial seasonal breakage and dislodgment (Seymour et al., 1989; Dudgeon and Johnson, 1992; Dudgeon et al., 1999; Johnson, 2001; Pratt and Johnson, 2002), presumably due to wave-induced forces. For example,

for two turf-like intertidal macroalgae, Dudgeon and Johnson (Dudgeon and Johnson, 1992) observed wintertime reduction in canopy cover reaching 13% for one species and 30% for another. In kelp forests, Seymour et al. (Seymour et al., 1989) documented mortality ranging from 2 to 94% over four winter seasons. And the sometimes meter-deep piles of seaweed washed up on beaches after storms stand testament to frequent breakage and dislodgment.

Failure in seaweeds assumes a variety of forms. For example, breakage of blades or load-bearing midribs may occur primarily at distal or marginal regions. This 'tattering' reduces the sizes of algal thalli (Black, 1976; Blanchette, 1997; Dudgeon et al., 1999) and presumably lowers the risk of more catastrophic damage. Other seaweeds, especially those with perennial holdfasts capable of regenerating stipes, break primarily at the holdfast-stipe junction (Carrington, 1990; Hawes and Smith, 1995; Shaughnessy et al., 1996; Carrington et al., 2001; Johnson, 2001). For instance, when experimentally pulling a turf-like red macroalga, Carrington (Carrington, 1990) found that 90% of thalli broke at the stipe-holdfast junction. Failure of this weak link ensures survival of the holdfast and allows regeneration of stipes and blades. Nonetheless, holdfast dislodgment, due to holdfast or substratum failure, does occur frequently (Black, 1976; Koehl, 1986; Seymour et al., 1989; Utter and Denny, 1996; Gaylord and Denny, 1997). For feather-boa kelp (*Egregia laevigata* Setchell) washed onto beaches, Black (Black, 1976) documented dislodgment due to holdfast or substratum failure for 35% of individuals, and Koehl and Wainwright (Koehl and Wainwright, 1977) determined holdfast detachment responsible for 3–55% of dislodged and broken individuals of a subtidal kelp, *Nereocystis luetkeana* (Mertens) Postels & Ruprecht, with tangled plants more likely to fail at the holdfast.

In sum, although wave-swept macroalgae appear over-designed on the basis of measured algal strengths and maximal wave-induced stresses, breakage nonetheless occurs commonly at various locations on macroalgal thalli.

To account for the discrepancy between predicted and observed algal breakage rates, several external factors, aside from maximum water speeds, have been invoked. Studies have suggested that stipe entanglement, low-tide physiological stress, senescence, water-propelled projectiles, and damage from herbivory or abrasion may increase breakage beyond rates predicted on the basis of maximum water velocities alone (Friedland and Denny, 1995; Utter and Denny, 1996; Kitzes and Denny, 2005; Denny, 2006). Along these lines, two studies, for two different kelp species, linked herbivorous damage to breakage in approximately 30–50% of solitary individuals washed ashore (Black, 1976; Koehl and Wainwright, 1977), and for the subtidal kelp *N. luetkeana*, Koehl and Wainwright (Koehl and Wainwright, 1977) observed breakage at abraded locations on thalli in approximately 40% of solitary individuals cast ashore. In addition, various researchers have speculated that *repetition* of wave-induced stress, not just the maximum stresses, may contribute to algal breakage (Koehl, 1986; Hale, 2001; Kitzes and Denny, 2005). Experiencing in excess of 8000

waves per day, each with imposition of rapid flow variation (Gaylord, 1999), intertidal macroalgae may be weakened by the repeated loading of stresses too low to break them in pull-to-break tests.

In this primer, we focus on the potential role of repeated loads in mechanical failure of wave-swept algae. Repeated loading may act in concert with damage initiated by abrasion and herbivory to cause breakage and dislodgment by fatigue.

The role of fatigue

Repeated stresses contribute to breakage in several ways. Through fatigue processes, wave-induced stresses below ultimate strength may cause formation of cracks, originating from existing material defects. Although the potential importance of fatigue crack initiation has been cited (Koehl, 1984; Koehl, 1986; Hale, 2001; Kitzes and Denny, 2005), fatigue has not been evaluated in macroalgae. Once a crack has formed in an alga through fatigue, herbivory or abrasion, it can locally amplify stress, thereby decreasing the alga's ultimate strength (where strength is calculated from bulk force applied to a specimen, disregarding local amplifications) and rendering the alga more susceptible to breakage by the imposition of a single large stress (e.g. Black, 1976; Johnson and Mann, 1986; Armstrong, 1987; Biedka et al., 1987; Denny et al., 1989; Lowell et al., 1991; DeWreede et al., 1992). Even if an alga containing a crack does not experience stress sufficient to break it in a single loading, repeated stresses below the alga's ultimate strength may cause a crack to grow to a length at which breakage occurs (Hale, 2001). In other words, repeated wave stresses that never reach a cracked alga's ultimate strength may cause fatigue crack growth to the point of complete fracture.

Most structural failures in human construction result from stresses well below the ultimate material strengths of building materials. Consequently, engineering theory includes a robust literature on crack formation through fatigue and on growth of cracks introduced by fatigue or other means. We focus specifically on fracture mechanics theory relevant to crack growth. Fatigue has been evaluated, but not with fracture mechanics methods, in biological materials ranging from bone to elastic proteins (e.g. Caler and Carter, 1989; Currey, 1998; Keaveny et al., 2001; Gosline et al., 2002). Failure in the presence of cracks has been assessed using fracture mechanics in biological materials such as bone, shell, horse hoof and grasses (e.g. Behiri and Bonfield, 1984; Bertram and Gosline, 1986; Vincent, 1991; Kasapi and Gosline, 1996; Kuhn-Spearing et al., 1996; Kasapi and Gosline, 1997; Currey, 1998; Taylor and Lee, 2003). However, these biological studies involving fracture mechanics have focused on the parameters relevant to propagation of cracks when materials fail catastrophically in response to single loadings. Although gradual crack extension may eventually cause complete fracture in conditions of repeated loading, few biological studies have examined incremental crack growth at sub-critical repetitively applied loads. Thus, studies to date do not address

our central question: can repeated loading of seaweeds lead to their breakage?

Literature regarding fracture mechanics is almost exclusively written for specialized engineering audiences, and deciphering it, with the aim of applying it to biological situations, remains difficult for most biologists and even for many engineers. In response to the opacity of fracture mechanics literature, we provide here a coherent primer as a starting point for studies of fracture in organisms and as a strong basis for further investigation of the literature. To this end, we present a guide to relevant fracture mechanics techniques. We use consistent terminology for various fracture mechanics methods (a luxury often absent in the literature) and introduce relevant equations with intuitive explanations instead of extensive derivations. Interested readers are guided to cited literature for more detailed descriptions of equations' origins.

Although we use macroalgae as organisms of focus, presented techniques have been applied, at least in part, to biological materials such as bone and horse hoof (Behiri and Bonfield, 1984; Bertram and Gosline, 1986; Kasapi and Gosline, 1997; Currey, 1998) and are relevant to more extensible, softer biological materials such as cnidarian mesoglea, arterial wall, skin, tendon and muscle (Purslow, 1989). We discuss applied wave forces, but imposed stresses from any source can cause repeated-loading damage. The accompanying article (Mach et al., 2007) tests the feasibility of applying these techniques to several macroalgae.

We begin with two central parameters in linear elastic fracture mechanics (LEFM), stress intensity factor and strain energy release rate, describing use of these parameters as background for our presentation of techniques relevant to flexible, extensible materials. [Readers interested in applying LEFM techniques to botanical materials are referred to Farquhar and Zhao (Farquhar and Zhao, 2006).] We then discuss strain energy release rate as it has been applied to fracture and incremental crack growth in highly extensible elastomeric materials. Finally, we discuss another parameter, the *J*-integral, that has been effective in characterizing fracture and fatigue in materials not well described by LEFM and fracture mechanics of elastomers.

For each fracture mechanics approach, we describe the methods used to evaluate the lifetime of a material with a crack of a particular size. That is, presented parameters enable estimation not only of the force necessary to fracture a specimen in a single loading, but also of the number of smaller repeated loadings that would eventually lead to fracture through incremental crack growth. We hypothesize that, by quantifying the effects of repeated loadings in this manner, we will be better able to predict algal breakage on wave-swept shores.

Cracks reduce strength

The stress intensity factor (linear elastic fracture mechanics)

If you attempt to open a bag of peanuts by pulling on the bag in tension, you will likely have trouble tearing the plastic.

Notch a side of the bag with scissors, and it will tear with ease. The same phenomenon occurs with seaweeds. Notches – in the form of cracks or discontinuities of any sort – reduce strength (calculated from bulk applied force) because they concentrate stress at their tips (e.g. Andrews, 1968; Shigley and Mischke, 2001). In other words, the material at a crack tip experiences local stresses that exceed the applied stress in the bulk of the specimen. In this fashion, failure may originate at the crack tip even when the bulk stress applied to the rest of the material is not sufficient to cause breakage. Once failure starts, the crack can propagate through the material. As the crack increases in length, it concentrates more stress at its tip, causing crack growth to accelerate and further decreasing the specimen's strength (Broek, 1982).

In the following sections, we consider several types of stress–strain behavior, depicted in Fig. 1, where strain is the ratio of change in length to original length as stress is applied to a material (engineering strain). Linear elastic stress–strain behavior refers to materials with linear relations between stress and strain that return to their original length when unloaded (Fig. 1A). Non-linear elastic materials also recover deformations upon unloading but display non-linear relations between stress and strain (Fig. 1B). Finally, elastic–plastic materials, upon loading, exhibit non-linear relations between stress and strain but additionally, upon unloading, leave irreversible deformation, termed plastic strain (or permanent set) (Fig. 1C). This plastic deformation exemplifies an inelastic strain.

First, we consider linear elastic fracture mechanics (LEFM). Although linear elastic material behavior may not characterize most seaweeds, LEFM provides basic fracture concepts and background information helpful in presenting other fracture mechanics approaches described here.

Stress intensity factor is a parameter that, for linear elastic materials, characterizes stress fields at very sharp crack tips. As an example, for a sheet with an edge crack experiencing bending or axially applied stress (Fig. 2A), the stress intensity factor, K_I (measured in Pa$\sqrt{m}$), can be expressed as:

$$K_I = \sigma \sqrt{\pi a}\, f\left(\frac{a}{w}\right),\qquad(1)$$

where σ is the bulk tensile stress applied to the sheet, computed as if no crack were present; a is a measure of crack length; w is the width of the specimen; and $f(a/w)$ is a dimensionless function of the crack geometry and sheet width. For derivation and further description of Eqn 1, see elsewhere (Broek, 1982; Broek, 1989; Atkins and Mai, 1985; Saxena, 1998). $f(a/w)$, often theoretically derived, assumes various forms (Saxena, 1998; Anderson, 2005). Eqn 1 can be applied to a variety of specimen and crack geometries with appropriate relations for $f(a/w)$, as given in Saxena (Saxena, 1998), Anderson (Anderson, 2005) and other sources. As a straightforward example, for a center-cracked sheet (Fig. 2B) with dimensions much larger than crack length, $f(a/w)=1$ (Broek, 1982; Anderson, 2005), and:
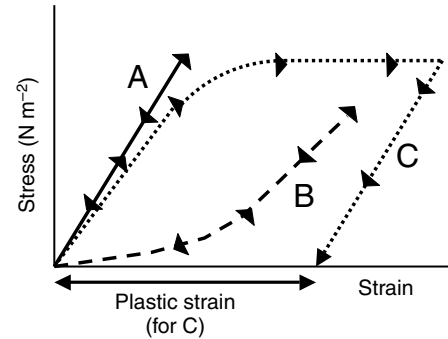
$$K_I = \sigma \sqrt{\pi a}\,.\qquad(2)$$

Fig. 1. Schematic showing different types of stress–strain behavior: (A) linear elastic, (B) non-linear elastic and (C) elastic–plastic with unloading.
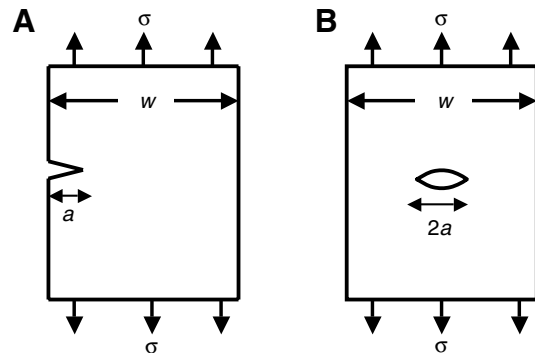

Fig. 2. (A) Edge-cracked sheet experiencing bulk tensile stress σ, with crack length a and width w. (B) Center-cracked sheet with crack length denoted as $2a$ for reasons related to mathematical derivation of the corresponding stress intensity factor.

The subscript 'I' of K_I indicates that this parameter refers to mode I loading, illustrated in Fig. 3A. Although mode I loading is depicted for a specimen with a single edge crack (Fig. 3A), a sample with a central crack (Fig. 2B), for example, pulled in tension will also experience mode I, tensile-opening loading. Although seaweeds may experience some mode II (Fig. 3B) and mode III (Fig. 3C) loading, many of the imposed loads on seaweeds can be approximated as mode I, tensile-opening loading. Accordingly, we predominantly address this first loading mode, not giving analogous equations for other loading modes.

LEFM was originally developed for application to metals, in which concentrated stresses near crack tips cause plastic (permanent) deformations in tip vicinities. As long as plastic deformations are confined to a small zone around the crack tip, LEFM stress intensity factors, as well as strain energy release rate expressions described in the next section, can be applied to metals and other materials.

The critical value of stress intensity factor, K_I, at which cracks advance is termed fracture toughness, K_C. This critical

A   **B**   **C**
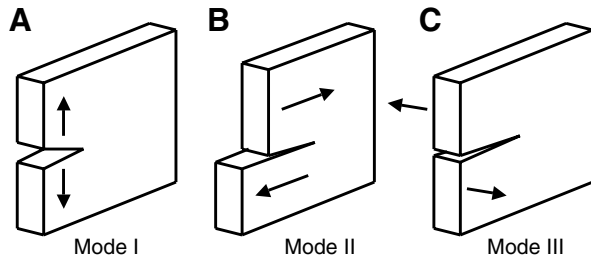
Mode I   Mode II   Mode III

Fig. 3. Three loading modes of cracked specimens: (A) mode I: tensile opening (cleavage); (B) mode II: in-plane shearing; and (C) mode III: anti-plane shearing (tearing).

value of stress intensity factor does depend on loading mode; K_C here denotes fracture toughness for mode I loading. K_C can be considered a material property in that it characterizes strength in the presence of a crack. As with properties such as ultimate tensile strength (breaking stress), fracture toughness typically varies with factors like temperature and rate of load application. For a given material, K_C is approximately constant for different combinations of crack lengths and applied stresses, as well as for different specimen geometries, such as the examples shown in Fig. 2. K_C is determined, using a relation such as Eqn 1, by measuring breaking stress for a material specimen of known dimensions, geometry and crack length. Once determined for one combination of specimen and crack geometry, K_C can be applied to assess resistance to cracking for other geometries of the material.

With units of $Pa\sqrt{m}$, stress intensity factors may seem abstract. A comparison between applied stress and stress intensity factor may thus be helpful. When a specimen with no crack is loaded, stress applied to the material can be measured easily. If the loaded sample breaks in two, the stress at failure is a measure of ultimate tensile strength. When the material contains a crack, however, due to variation of stresses within the sample, the applied stress at failure will no longer be constant for the material. Instead, stress at failure will vary with size and shape of the crack as well as with geometry of the test specimen, with geometry determined by relative specimen dimensions and crack location. Consequently, in the case of a cracked specimen, stress intensity factor, K_I, instead of simply applied stress, can be used to describe the physical state of the material. If the loaded sample breaks in two, the pertinent parameter becomes not applied stress at fracture, but stress intensity factor at failure, which is called fracture toughness, K_C. Thus, this geometry-independent term (fracture toughness) is the material property preferred for characterizing loading in materials with cracks.

Once determined for one combination of specimen geometry and crack size (and given linear elastic conditions with limited crack-tip plasticity), fracture toughness can be used to assess the reduction in a material's strength for different specimen geometries and crack sizes. For tensile-opening, mode I loading

(Fig. 3A), the strength of the material, σ_C, is reduced by the presence of a crack according to:

$$\sigma_C = \frac{K_C}{\sqrt{\pi a}\, f\left(\dfrac{a}{w}\right)}, \qquad (3)$$

where a is crack size and $f(a/w)$ is selected appropriately for the specimen and crack geometry of interest (Broek, 1989; Saxena, 1998). In other words, given fracture toughness, strength of a specimen with known crack length can be predicted.

LEFM, which includes stress intensity factors and strain-energy-release-rate expressions described below, performs best for materials such as glass and ceramics, which have little or no ability to deform plastically and which have high moduli of elasticity (i.e. they are stiff materials) and therefore experience relatively small bulk strains when loaded to fracture. (Modulus of elasticity is the slope of a stress–strain curve, with units of $N\,m^{-2}$.) For such materials, strength reduction can be predicted reliably with Eqn 3. For seaweeds, however, large deformations act to round the crack tip and reduce stress concentrations, thereby limiting the utility of linear elastic expressions in predicting strength reduction in the presence of cracks (Biedka et al., 1987; Denny et al., 1989; DeWreede et al., 1992). Crack-tip rounding ameliorates the strength reduction predicted by Eqn 3. Nonetheless, cracks of various geometries have been demonstrated to increase the likelihood of breakage in several macroalgae (Denny et al., 1989; DeWreede et al., 1992).

In summary, stress intensity factor K_I characterizes the stress field at a crack tip for linear elastic behavior, and fracture toughness K_C quantifies the critical value of this factor at which a crack will propagate unstably to failure. Higher fracture toughness values occur in materials more resistant to fracture in the presence of cracks.

Crack propagation

Energy considerations (linear elastic fracture mechanics)

Crack propagation can also be examined in terms of energy (Broek, 1982; Broek, 1989). When a material specimen is pulled, work is done on the sample. In this case, work is force multiplied by specimen displacement, where displacement is specimen current length minus specimen initial length. If a sample is pulled to an extension and held, work is no longer done on the sample, but the sample still contains energy – as evident, for example, in a stretched rubber band flying across a room when released. This energy stored in the material is strain energy, U.

Consider a laboratory sample of an elastic material held by grips and pulled in tension to a fixed displacement. This fixed-grip condition can be used to explain another important concept: 'strain energy release rate'. Work expended in extending the sample is stored as elastic strain energy, U, and no further work is done once the grips are stationary. Assuming no dissipative energy loss (e.g. through heat), the density of this stored energy, the elastic strain energy density ($J\,m^{-3}$), equals

the area under the material's stress–strain curve at the fixed strain imposed by the grips.

Now, imagine introducing a sharp slit (or crack) into this extended fixed-grip specimen. When the crack extends incrementally, creating new crack surface dA, strain energy in material around the crack will relax, causing the elastic energy stored in the specimen to decrease by dU. This decrease in stored energy as new crack surface forms is known as the strain energy release rate, G (J m^{-2}), given by:

$$G = -\frac{dU}{dA} . \qquad (4)$$

Note that energy release rate is defined with respect to crack area, not time, unlike other common rates such as velocity. Crack surface area, A, is not to be confused with crack length, a. Crack area A is calculated as crack length multiplied by specimen thickness.

Some confusion in biological literature has arisen due to differing definitions of dA (Biedka et al., 1987; Denny et al., 1989; Hale, 2001). Sometimes new crack surface area created in crack extension is taken to include surface area of both faces of the crack, while at other times it includes surface area on only one face of the crack. Here, dA refers to newly created surface area on one face of the crack, and we encourage use of this convention to standardize measurements.

For a central crack in a sheet (Fig. 2B) with length and width much greater than crack size, evaluating Eqn 4 for mode I loading gives strain energy release rate as:

$$G_I = \frac{\pi\sigma^2 a}{E} , \qquad (5)$$

where σ is the bulk stress applied to the specimen, a is half the length of the central crack, E is the elastic modulus of the material, and subscript 'I' again indicates mode I, tensile-opening loading (Broek, 1982; Perez, 2004; Anderson, 2005).

Fracture testing usually involves pulling a cracked specimen while recording force-*versus*-displacement data. In such cases, strain energy release rate can be evaluated at displacements selected by the analyst, applying an experimental procedure similar to that introduced in Appendix A.

A crack will extend in a material when strain energy released in crack growth (expressed as a rate, dU/dA) exceeds energy required for the increase in crack surface area, dV/dA. The energy, V, absorbed during crack extension includes energy to create new surface as well as any energy dissipated through plastic deformation at the crack tip. The per-area rate at which energy is required for creation of crack surface, dV/dA, is often termed crack resistance, R.

Crack extension occurs when strain energy release rate, G, reaches a critical value G_C equal to R. This crack advance may be stable or unstable. For example, when the driving force, G, for crack extension increases with crack growth, but crack resistance R remains constant, unstable growth occurs, which means that, once it begins to elongate, a crack will grow to specimen fracture. However, when R increases more than G with crack extension, stable crack growth occurs, in which

crack extension occurs but does not lead to specimen fracture. In this scenario, a crack can advance a certain distance (while $R<G$) and then stop (when $R>G$), until higher loads are applied. Stable crack advance occurs mainly in materials that produce large plastic deformations with crack extension, such as thin plastic grocery bags, for which crack edges ruffle significantly during tearing, indicating plastic deformations. In most cases, G_C, the critical strain energy release rate, corresponds to onset of unstable growth and fracture. Although we have described G here in terms of stationary grips to explicate the concept, G_C in practice is usually determined by pulling specimens with initial cracks until unstable crack extension occurs.

We thus arrive at two different criteria for rapid crack propagation. First, the stress intensity factor, K_I, must equal fracture toughness, K_C. Second, the energy release rate, G_I, must have reached its critical value, G_C. For linear elastic materials, these criteria are equivalent. From Eqn 2 and Eqn 5, we can deduce that:

$$K_I = \sqrt{G_I E} \qquad (6)$$

and at fracture,

$$K_C = \sqrt{G_C E} . \qquad (7)$$

These relations remain valid for different crack and specimen geometries. Thus, for linear elastic materials, the reduction of material strength in the presence of a crack can be assessed through either of these criteria. Knowing K_C yields G_C, and *vice versa*. K_C and G_C are properties of a given material, so for a crack of length a, the stress σ required for fracture in the presence of this crack can be derived either by the stress-intensity-factor approach (Eqn 1 or Eqn 2) or by the strain energy release rate approach (Eqn 4 or Eqn 5).

Fatigue crack growth

Techniques from linear elastic fracture mechanics

We now discuss a crucial point. As we have just noted, for a material with a crack, applied stress must reach a critical value corresponding to K_C or G_C for crack extension to occur. In a given specimen, longer cracks require lower applied stresses to propagate (Eqn 3). However, *for repeatedly applied stresses resulting in sub-critical values of K_I and G_I, crack growth can still occur, in a very slow, incremental manner*. In conditions of repeated loading, incremental fatigue crack growth at sub-critical K_I and G_I can result in gradual growth of a crack to a length at which it does rapidly propagate, fracturing the material.

In other words, for a macroalga with a crack, wave forces causing stresses less than the material's ultimate strength in the absence of cracks, and less than the applied stress required for complete fracture, may still cause crack growth (that is, small increases in crack length) with each force imposition. At a certain point, the alga's crack may grow to a length at which applied wave forces reach G_C and K_C, leading to the fracture described in the previous sections. As a result, examining algal fracture in a manner that considers only maximum wave forces may neglect breakage that will occur due to incremental crack

growth during smaller, repeated loadings. The curious, important phenomenon of 'sub-critical' crack growth can be characterized (although not mechanistically explained) using the following LEFM procedure, which allows prediction of a material's lifetime in conditions of repeated loading. The physical mechanisms for incremental crack growth have been documented for some engineering materials but not for macroalgae. For metals, for example, when a crack opens in response to sub-critical bulk stresses, localized plastic straining at the crack tip causes the tip to blunt on a microscopic scale, which elongates the crack a small amount. Upon removal of the bulk stress, the crack tip re-sharpens with increased length, iteratively elongating with repeated loading (Pook, 1983).

Predictions of specimen lifetimes proceed in two steps. First, baseline data are generated to describe the pattern of crack growth in a material. This baseline curve (Fig. 4) is then combined with real-world loading histories to predict time to failure.

Baseline curve

To create a baseline curve of crack growth, tests are conducted on samples of a given material with different initial crack sizes or different imposed stresses. For example, samples can be loaded with stress varying sinusoidally from zero to a maximum value, with concurrent observation of increases in crack length, a, as a function of cycle number, N. Note that a cycle of imposed stress corresponds to the period spanning from maximum imposed stress, to minimum imposed stress, and back to maximum imposed stress. Repeated cyclic loading is often imposed on a specimen, with periodic measurement of crack length, until the sample fractures. The magnitude of stress range imposed (maximum stress minus minimum stress) generally exerts the greatest influence on crack growth rates, as compared to loading characteristics such as cycling frequency.

From a curve fitted to *a-versus-N* data, crack growth rates (mm cycle^{-1}), *da/dN*, are calculated from the curve's slope at different values of crack length, a. For each value of crack length, a range of stress intensity factor, ΔK_I, is computed from the range of applied stress, $\Delta\sigma$ (maximum stress minus minimum stress in a cycle), using a relation such as Eqn 1. If the minimum stress is zero, then ΔK_I equals the maximum value of K_I applied in a cycle.

Crack growth rate values, *da/dN*, are then plotted against values of stress intensity range, ΔK_I, on logarithmic axes, where ΔK_I (for cyclic loading from zero to maximum stress) equals the value of the stress intensity factor, K_I, at the maximum imposed stress (Fig. 4). Each material has a characteristic log–log plot of *da/dN versus* ΔK_I, which often has the shape depicted in Fig. 4. Growth rate generally increases with increasing crack length and with increasing applied stress. At low ΔK_I, crack growth is extremely slow, and there is sometimes a threshold value of ΔK_I below which no crack growth occurs (Broek, 1982), shown as ΔK_{TH} in Fig. 4. Similar baseline curves can be generated for other loading modes (Fig. 3) as well.
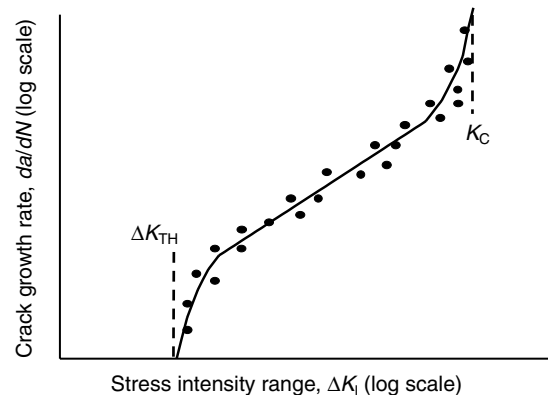

Fig. 4. A log–log plot illustrating patterns of crack growth for conditions of repeated loading. Crack growth rate (mm cycle^{-1}), *da/dN*, indicates the increase in crack length for each cycle, N, of sinusoidally varying applied stress. Stress intensity range (Pa$\sqrt{\text{m}}$), ΔK_I, indicates the variation in stress intensity factor during each cycle of loading. ΔK_{TH} indicates threshold stress intensity factor range, and K_C denotes fracture toughness.

Lifetime

Once baseline data are generated, lifetime of a cracked material in repeated loading conditions can be determined. Determination of lifetime requires a loading history, a plot of stress applied to a material over time. The loading history is analyzed to predict when fracture will occur, that is, when K_C or G_C will be reached. There are multiple approaches to this calculation. In one common LEFM approach, crack growth is assumed to occur only during rising, tensile ranges of loading (Nelson, 1977). In other words, crack growth is assumed to occur only while applied stress stretches a specimen beyond its initial length, not while specimen extension decreases in tension and not while a specimen is loaded in compression. In the loading history, each time that applied tensile stress increases from one value to another and then drops, that increase (or range) of stress is considered equivalent to a loading cycle used in generation of the baseline *da/dN-versus-*ΔK_I curve (Fig. 4).

For each successive rising tensile range in a loading history or in a representative sequence of loading, crack growth for that cycle is added to current crack length. The increment of crack growth for the cycle, *da/dN*, corresponds, on the baseline data plot (i.e. Fig. 4), to the stress intensity range ΔK_I of the tensile loading. As subsequent stress impositions are analyzed, crack length increases, and when the stress intensity range reaches fracture toughness, fracture is predicted to occur. In other words, the critical crack length corresponding to G_C or K_C for the applied stress has been reached, and material rupture is predicted, as long as resistance to fracture, R, does not increase significantly with crack extension, as described in the previous section. In this fashion, the number of loadings to failure, or lifetime, of the cracked material is estimated.

In sum, to apply this procedure to a seaweed, one experimentally generates a baseline curve describing crack

growth in response to repeated loading in a macroalga containing cracks, i.e. a log–log da/dN-versus-ΔK_I curve (Fig. 4). Each species, and perhaps each population, requires a separate baseline curve characterizing its crack growth behavior. Then a history of imposed wave forces is converted to imposed wave stresses through consideration of a macroalga's cross-sectional area. For each rising tensile imposition of stress in this wave stress history, the calculated range of applied stress, $\Delta\sigma$, combined with crack length, a, can be used to determine ΔK_I for the loading (e.g. Eqn 1). Then, for each rising stress imposition, the corresponding crack growth is determined from ΔK_I for the stress imposition and from the corresponding da/dN in the baseline data curve. When crack length is sufficient for ΔK_I to equal K_C, breakage of the alga is predicted.

The power of this procedure is that breakage of seaweeds can be examined in a manner that considers each force imposition (each wave) that seaweeds experience. It thus estimates the lifetime of a cracked alga as number of waves required for a crack to grow to failure.

In general, crack growth in engineering materials involves substantial variability (Broek, 1982), and differences between predicted and actual growth result from variability in material cracking and fracture behavior, as well as from idealizations and simplifications in prediction methods. Similar variability likely occurs for macroalgae.

LEFM may not effectively characterize algal fracture. Because LEFM performs best for materials displaying brittle fracture (which seaweeds often do not, compared to engineering materials), alternative methods should be explored, and two such approaches are described below. Even if other methods are found superior for application to seaweeds, LEFM might be well applied to some plant materials such as leaves and wood (Farquhar and Zhao, 2006) or to shells to predict cycles to failure during predator loadings (e.g. Boulding and LaBarbera, 1986; LaBarbera and Merz, 1992) or wave force impositions.

Crack growth in macroalgae

Fracture mechanics of elastomeric materials

Macroalgae generally exhibit high extensibility and non-linear stress–strain curves (e.g. Fig. 5), factors that potentially limit the utility of LEFM techniques in analyzing and predicting fracture in seaweeds. However, these characteristics of seaweeds (along with their incompressibility) are similar to the properties of rubber and other elastomers, and a common modified approach to fracture mechanics designed for elastomers is likely applicable to seaweeds.

Based on energy considerations, Rivlin and Thomas (Rivlin and Thomas, 1953) pioneered the fracture mechanics of rubber-like materials. They demonstrated that Eqn 4 for strain energy release rate can be applied to such materials. Their approach does not assume linear stress–strain behavior, but does presume elasticity. This presumption is often approximately true in regions far from crack tips (i.e. not at stress concentrations) in
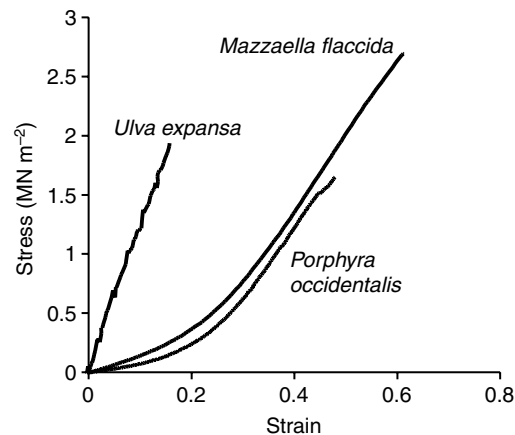

Fig. 5. Representative stress–strain curves for pull-to-break tests of three macroalgae (Hale, 2001).

rubber or macroalgal specimens. Furthermore, their methods can be applied when bulk strains are large, even 100% or more, which involves a doubling of specimen length during loading (Lindley, 1972). To be consistent with their nomenclature, and that of subsequent researchers in fracture mechanics of elastomers, when discussing this approach we denote strain energy release rate as T instead of G.

Strain energy release rate, T, may be found experimentally, as for linear elastic materials, by loading specimens with initial cracks until cracks extend unstably (Appendix A). Critical values of T_C defined by these loadings are analogous to G_C for linear elastic materials. Experimental results demonstrate that T_C is approximately constant for different specimen and crack geometries and therefore can be considered a material property characterizing resistance to fracture (Rivlin and Thomas, 1953; Thomas, 1994). Thomas (Thomas, 1955; Thomas, 1994) also showed that T can be related to W, the strain energy density around the surface of a crack tip of diameter d:

$$T = d \int_0^{\frac{\pi}{2}} W(\theta)\cos\theta \, d\theta , \qquad (8)$$

where θ is the angle shown in Fig. 6 and $W(\theta)$ indicates that W is a function of θ. Thomas determined this relation by considering a specimen's change in energy with an increment of crack extension, which is dominated by elastic strain energy relaxed in a small zone ahead of the crack tip (Thomas, 1994). Derivation of Eqn 8 assumes elastic, including non-linear elastic, behavior and strains less that 200% (Thomas, 1955). This equation indicates that blunting of a crack tip, which increases crack-tip diameter d, can thus be expected to increase values of T_C.

Fortunately, relatively simple analytical expressions for T have been derived for a number of important specimen types. These expressions also assume elastic stress–strain behavior and permit substantial bulk strains. We briefly describe relevant equations without detailing corresponding derivations. We refer the reader to cited sources for derivations.
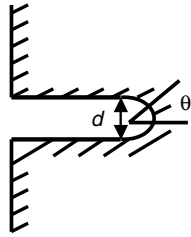
Fig. 6. Schematic of a rounded crack tip with diameter d and angle θ.
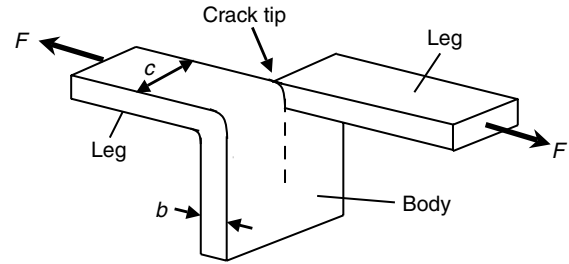

Fig. 7. A trouser test piece after a crack has extended from an initial incision. The path of future crack growth is shown as a broken line. Force F is applied to both legs. Each leg has width c, and legs and body have thickness b. Cross-sectional area of the test piece, C, equals $b \times 2c$.

Single-edge-crack specimens

For rubber specimens each with a single edge crack (e.g. Fig. 2A), pulled in tension, energy release rate is given by:

$$T_I = 2kW_o a \,, \tag{9}$$

where W_o is strain energy density (that is, energy per unit volume) present in the bulk of the specimen and k is a parameter related to specimen extension, with extension expressed as an extension ratio λ (Rivlin and Thomas, 1953; Lake, 1983). Extension ratio is simply a ratio of a specimen's current length to its initial length. That is, an extension ratio of 2 corresponds to strain of 1, or a doubling in length. Eqn 9 assumes an incompressible elastic material and crack sizes small compared to specimen width. Greensmith (Greensmith, 1963) found experimentally that k is approximately π at $\lambda=1$, then drops to approximately 1.6 at $\lambda=3$. Numerical analysis confirmed these results (Lindley, 1972). Variation of k with λ can be adequately approximated by the simple relation:

$$k = \frac{\pi}{\sqrt{\lambda}} \,. \tag{10}$$

(Atkins and Mai, 1985; Lake, 1995; Seldén, 1995).

To determine critical energy release rate, T_C, a single-edge-crack specimen with crack length a is stretched until it breaks, and force and extension at fracture are measured. W_o in Eqn 9 can be found from the stress–strain curve of a specimen without a crack; W_o is the area under that stress–strain curve up to the bulk stress at which fracture occurred in the cracked specimen.

Trouser-tear specimens

Another common method for determining T_C of rubber-like materials involves trouser-tear specimens (Fig. 7). A trouser-tear specimen consists of a rectangular sheet cut along its long axis to form a pants-shaped test piece. The 'legs' are pulled in opposite directions to create tearing action (Fig. 3C). Greensmith and Thomas (Greensmith and Thomas, 1955) note the convenience of this test piece, for which T_C and rate of tear propagation are independent of crack length.

Ahagon et al. (Ahagon et al., 1975) indicate that crack growth in rubber trouser-tear specimens may actually occur on inclined planes such that tensile stresses applied to the legs act in a normal direction to the planes of cracking, which results in mode I cracking (Fig. 3A). On the other hand, Mai and Cotterell (Mai and Cotterell, 1984) and Joe and Kim (Joe and

Kim, 1990) note that trouser-tear testing of rubber may involve a mixture of mode I and mode III cracking. For thin sheets of biological materials, the mode or modes of cracking in trouser-tear testing are unclear at this time.

For trouser-tear tests, critical energy release rate can be found from:

$$T_C = \frac{2\lambda F}{b} - \frac{W_o C}{b} \,, \tag{11}$$

where λ is extension ratio in the legs during tearing, F is force applied to the legs during tearing, b is initial thickness of the test piece, W_o is strain energy density in the legs during tearing, and C is initial cross-sectional area of both legs combined, the cross-sectional area of the 'body' of the test piece (Rivlin and Thomas, 1953; Greensmith and Thomas, 1955; Lake, 1983). Often, extension of legs and strain energy stored in legs are assumed negligible relative to energy associated with crack extension (Rivlin and Thomas, 1953; Greensmith and Thomas, 1955; Seldén, 1995), in which case:

$$T_C = \frac{2F}{b} \,. \tag{12}$$

Thus, for trouser-tear specimens, critical values of T_C can be found by monitoring force required to propagate a crack. Another approach for finding T_C with this specimen type involves finding the net energy, Λ, expended in loading, tearing, and unloading of a specimen, obtained from the area under a force–displacement plot (e.g. Fig. 8). Then, critical energy release rate is given (Purslow, 1983) by:

$$T_C = \frac{\Lambda}{\Delta ab} \,. \tag{13}$$

where Δab is the crack extension surface area, taken as distance traveled by a crack between its initial and final lengths, Δa, multiplied by thickness of a specimen, b. Fluctuations in force with crack extension of the kind illustrated in Fig. 8 are typical of variations observed for macroalgae as well as other pliant biological tissues (Purslow, 1989).

Biedka et al. (Biedka et al., 1987) and Denny et al. (Denny et al., 1989) determined critical strain energy release rates for seaweeds from trouser-tear tests using formulations similar to
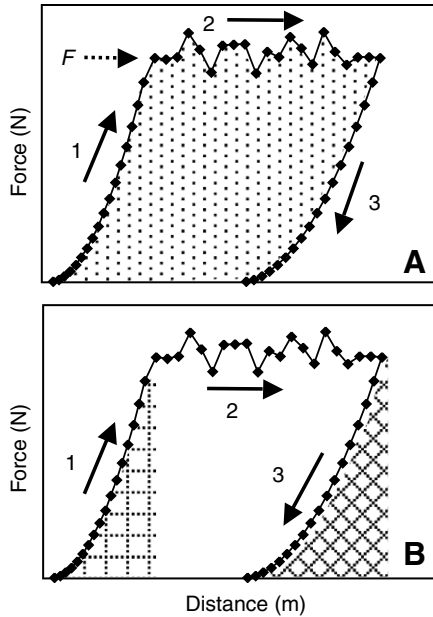
Fig. 8. Force applied to a trouser-tear test piece is plotted against distance of test piece's extension. Arrow 1 indicates the specimen's initial extension, arrow 2 indicates tearing of the test piece at average force F, and arrow 3 indicates final retraction of the specimen as applied force is removed. The stippled area in (A) depicts energy released in crack extension. In (B), hatched area 1, under the initial extension curve (arrow 1), indicates strain energy in legs before crack growth. Cross-hatched area 3, under the retraction curve (arrow 3), indicates strain energy stored in legs at the end of the test. Because legs are longer at the end of the test due to crack extension, final stored strain energy (area 3) is greater than initial stored strain energy (area 1).

Eqn 12 and Eqn 13 except that they referenced fracture energy to two times the fracture surface area. They termed the measured property 'work of fracture', even though they measured critical energy release rate. Multiplying their works of fracture by two (and again by two for Denny et al.'s values to account for a spurious factor introduced in their calculations) yields critical strain energy release rates for seaweeds comparable to calculations from Eqn 12 and Eqn 13.

Center-crack specimens

For another specimen geometry, a center-cracked specimen (Fig. 2B), strain energy release rate for tensile-opening loading (Fig. 3A) is given by:

$$T_I = \frac{\pi W_o (2a)}{\sqrt{\lambda}}. \qquad (14)$$

(Seldén, 1995; Yeoh, 2002). This relation resembles the formulation for single-edge-notch specimens (Eqn 9 and Eqn 10), with crack length a as defined in Fig. 2B. The parameter k (here $k = \pi/\sqrt{\lambda}$) varies, strictly speaking, for center-crack (Eqn 14) and edge-crack (Eqn 9 and Eqn 10) specimens because deformation of an edge crack is less constrained, as discussed, for example, by Sanford (Sanford, 2003). However,

the difference in k for these two specimen types is small compared to other sources of variability and is often ignored.

In the linear elastic case, Eqn 14 is equivalent to the LEFM expression for G (Eqn 5). Under elastic conditions, strain energy density, W_o, is area under a stress–strain curve. Under linear elastic conditions, this area under the curve, and thus strain energy density, equals $\sigma^2/2E$. In addition, for linear elastic conditions, specimen extensions are usually small compared to elastomer extensions, so that $\lambda \cong 1$. Substitution of these values yields

$$T_I = \frac{\pi \frac{\sigma^2}{2E} (2a)}{\sqrt{1}} = \frac{\pi \sigma^2 a}{E} = G_I .$$

Therefore, in the linear elastic case for a center-cracked specimen, T reduces to G in Eqn 5, demonstrating consistency of the approaches. Equivalency of T, which assumes elastic stress–strain behavior and permits substantial bulk strains, and G, which assumes linear elastic behavior, holds true for other crack and specimen geometries.

Effects of viscoelasticity

Many elastomers, as well as macroalgae, display some degree of viscoelastic behavior, a combination of elastic and time-dependent viscous stress–strain behavior. As such, they violate the assumption of elasticity inherent in the analyses so far.

Viscoelastic behavior is characterized, for example, by stresses relaxing if material is moderately stretched and held fixed or by inelastic (creep) strains developing if material experiences constant load over time. Under constant-amplitude, cyclic loading, viscoelastic behavior appears in loops formed by stress–strain curves for repeated loading and unloading cycles (e.g. Fig. 9, as compared to elastic behavior shown in Fig. 1A,B). Viscoelastic loading–unloading loops displayed by seaweeds (Fig. 9A) resemble loops exhibited by rubbers (Fig. 9B). Often, for elastomers and macroalgae, loop width decreases with repeated cycles and tends towards much smaller values for lower specimen extension (e.g. Fig. 9). In addition, a residual inelastic (plastic) strain may remain after the first cycle, but additional increments of residual strains often become negligible (Fig. 9). Similar stress–strain behavior has been observed in other plant tissue (Spatz et al., 1999) and in muscle of soft-bodied arthropods (Dorfmann et al., 2007). This viscoelastic behavior will be most pronounced in crack-tip regions where stresses and strains are much higher than in the bulk of the specimen.

In spite of such complexities in material behavior, range of energy release rate, ΔT, has been used successfully to correlate crack growth rate under zero-to-tension repeated loading in rubber (Lake, 1995; Seldén, 1995; Mars and Fatemi, 2003; Schubel et al., 2004; Busfield et al., 2005), much as ΔK has been used successfully in linear elastic analyses. Since the value of T at the maximum point of a load cycle is ΔT when the minimum point is zero (no extension), T will be used here without Δ.
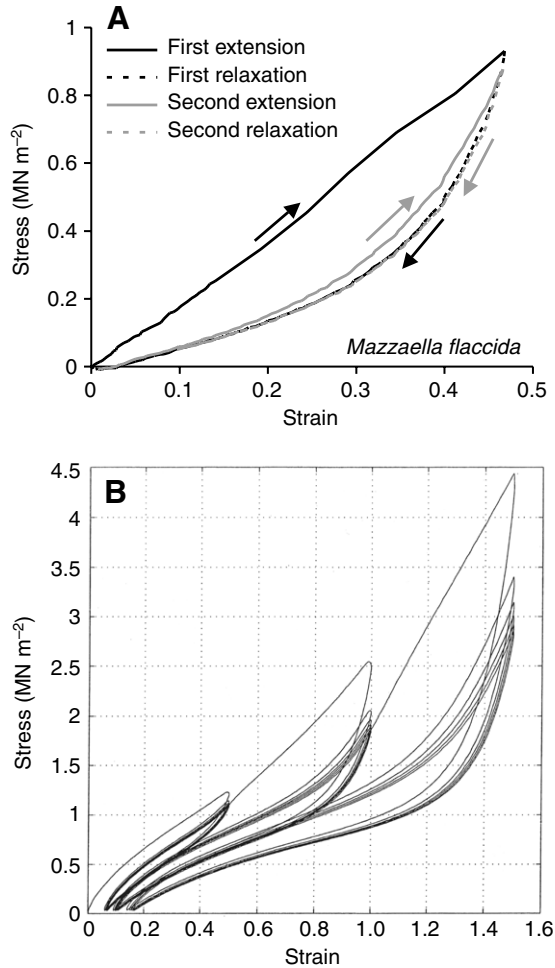
Fig. 9. (A) Stress–strain curves of a red macroalga, *Mazzaella flaccida* (Setchell & Gardner) Fredericq, for two cycles of stretching (Hale, 2001) showing a sizeable loading–unloading loop on the first cycle, followed by a much smaller loop on the second cycle. A small amount of residual strain remains after the first cycle. (B) Stress–strain curves, adapted from Dorfmann and Ogden (Dorfmann and Ogden, 2004), of a rubber compound for several cycles of stretching, showing similar stress–strain behavior, plus some reduction in maximum stress levels with cycling (stress softening). Curves are shown for maximum strains of 0.5, 1.0 and 1.5. Plot, copyright 2003, is reprinted with permission from Elsevier.

Characterizing crack growth rate

As with LEFM analyses, crack growth per cycle of loading, *da/dN*, may be evaluated in a nonlinearly elastic material over a range of strain energy release rates, *T* (Atkins and Mai, 1985; Lake, 1995; Seldén, 1995). Then, the relationship between *da/dN* and *T* is determined. The cyclic crack growth per cycle is represented as some simple function of *T*, a relationship often maintained over a wide range of crack growth rates:

$$\frac{da}{dN} = f(T) \,. \tag{15}$$

When *f(T)* is known, incorporating effects of specimen shape and applied forces, this equation can be used to predict crack growth rate behavior for a given material, analogous to data

presented in Fig. 4. For specimens each with a single-edge crack (Fig. 2A), cycled in tension, energy release rate is described by Eqn 9. For this equation, for a cyclically loaded sample, W_o is taken as the strain energy density at maximum extension, λ_{max}. W_o is often measured directly from stress–strain plots for un-notched samples, assuming that regions far from a crack behave as if no crack were present (Atkins and Mai, 1985). Likewise, *k* is calculated for λ_{max}. Calculated *T* is plotted *versus da/dN*, as done for ΔK_I data (Fig. 4).

For crack extension in regions of intermediate-to-high strain energy release rates, crack growth rate per cycle commonly follows an empirically determined power-law form (Lake, 1995; Seldén, 1995):

$$\frac{da}{dN} = BT^\beta \,. \tag{16}$$

Experimentally observed for a variety of rubbers, this relationship may aptly describe algal crack growth as well because of the resemblance between seaweed and rubber material behavior. B and β are constants fitted to *T-versus-da/dN* data. Once determined from tests using one set of crack sizes, *T* values, and particular specimen and crack geometry, these constants can be used in Eqn 16, for the same material, but for other crack sizes, *T* values and geometries.

Predicting lifetime

Eqn 16 can be integrated to determine the number of loading cycles, *N*, required for a crack to grow from length a_1 to length a_2. Consider the case of a single-edge-cracked specimen (Fig. 2A) that experiences cyclic loading with constant maximum extension. From Eqn 9, *T* in Eqn 16 is set equal to $2kW_oa$. Eqn 16 then becomes

$$\frac{da}{dN} = B(2kW_oa)^\beta, \quad \text{or} \quad \frac{da}{a^\beta} = B(2kW_o)^\beta dN \,.$$

For these loading conditions, $2kW_o$ assumes a constant maximum value because *k* and W_o are proportional to extension. One can then integrate

$$\int_0^N dN = \frac{1}{B(2kW_o)^\beta} \int_{a_1}^{a_2} \frac{da}{a^\beta} \,,$$

yielding (Lake, 1995; Seldén, 1995):

$$N = \frac{1}{(\beta-1)B(2kW_o)^\beta} \left(\frac{1}{a_1^{\beta-1}} - \frac{1}{a_2^{\beta-1}} \right) . \tag{17}$$

From this equation, the number of loading cycles required for an increment of crack growth can be determined. β often has a value of 2 to 6 (Lake, 1995). If, in addition, $a_2 \gg a_1$, the second term in parentheses in Eqn 17, $(1/a_2^{\beta-1})$, is negligibly small and can be dropped:

$$N = \frac{1}{(\beta-1)B(2kW_o)^\beta} \left(\frac{1}{a_1^{\beta-1}} \right). \tag{18}$$

In this way, the lifetime, in number of loading cycles, can be determined for a specimen with a small introduced crack.

This equation allows for powerful predictions [see accompanying article (Mach et al., 2007)]. Once baseline crack-growth behavior of an alga has been evaluated with Eqn 16, Eqn 18 can be used to estimate the number of waves of a certain magnitude required to break an edge-cracked alga through incremental crack growth. That is, for a flat-bladed alga with an edge crack, Eqn 9 can be used with stress–strain curves to determine the wave force required to fracture the alga in a single wave, once critical values of T have been measured. Eqn 18, in contrast, enables prediction of the wave force required to break an edge-cracked alga in, for example, 100, 1000 or 10 000 waves, thereby estimating lifetime of the notched alga in different wave conditions. Wave force can then be correlated with offshore wave height, given various assumptions about wave breaking (Gaylord, 1999; Denny et al., 2003; Helmuth and Denny, 2003; Denny, 2006), allowing predictions of the frequency with which notched algae experience waves sufficient to break them in these 100, 1000 or 10 000 wave loadings.

J-integral and elastic–plastic fracture

An important advance in the field of fracture mechanics was development of the *J*-integral (Rice, 1968a; Rice, 1968b), a line integral that evaluates the stress–strain field along a contour surrounding a crack tip (Fig. 10A). The *J*-integral is given in Appendix B. *J* and associated techniques have been applied successfully to assess fracture in the presence of cracks and to evaluate incremental crack growth even in specimens that experience substantial plastic deformation at crack tips or dissipative viscoelastic processes. This more flexible approach may have advantages for application to seaweeds as well as other biological materials (e.g. Bertram and Gosline, 1986).

J can be thought of as an energy-related parameter, the integral of two terms that contain strain energy density (or a product with units of strain energy density, $J\,m^{-3}$). Rice (Rice, 1968a; Rice, 1968b) derived *J* for non-linear elastic stress–strain behavior, and the integral is independent of the contour selected. The *J*-integral also characterizes intensity of strains in the crack-tip region, analogous in that respect to the stress intensity factor for linear elastic behavior. Computational and experimental methods for evaluating the integral are given in texts such as Kanninen and Popelar (Kanninen and Popelar, 1985), Saxena (Saxena, 1998) and Anderson (Anderson, 2005).

J has been found useful in analyzing resistance to crack extension in materials with extensive plastic deformation emanating from crack tips. The critical value of *J* at which onset of crack extension occurs, J_C, can be considered a material property. Like fracture toughness K_C, J_C is in principle independent of specimen and crack geometry as well as crack size. Over the years, *J* has been applied successfully as a fracture parameter for metals and plastics (Kim et al., 1989; Bose and Landes, 2003; Wainstein et al., 2004).

J can be interpreted graphically (Fig. 11). Suppose test specimens with two different crack lengths, a and $(a+da)$, are
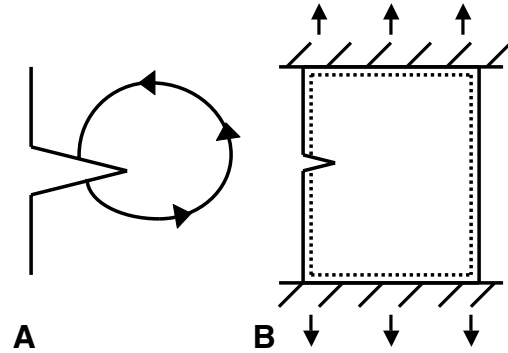

Fig. 10. (A) Diagram showing an integration path (contour) taken in a counterclockwise direction around a crack tip. (B) An edge-cracked specimen stretched and held with fixed displacement, showing a contour taken around the boundaries of the specimen.

pulled to a fixed displacement. The area between the curves for two different crack lengths (Fig. 11) represents the change in stored energy, dU, that occurs for crack extension da. dU is ($Jtda$), where t is specimen thickness and $dA=tda$ (Broek, 1982). For this fixed displacement example,

$$J = -\frac{dU}{dA}. \qquad (19)$$

The *J*-integral, despite its apparent complexity (Appendix B), is equivalent to G and T, given certain assumed material behaviors. For example, if the path (contour) for the *J*-integral is taken around the boundaries of an edge-cracked specimen (Fig. 10B), evaluation of *J* for rubber-like materials produces results equivalent to Eqn 9 (Oh, 1976). In this scenario, $J_I=T_I=2kW_oa$. Furthermore, calculating a *J*-integral for a rounded crack tip (Fig. 6) with the contour taken around the surface of the crack tip yields an expression equivalent to Eqn 8 for T. Also, if linear elastic behavior is considered, J_I can be shown to equal $(K_I)^2/E$, which by Eqn 6 is G_I (Rice, 1968a; Rice, 1968b).

Note that energy release rate usually involves energy released from a specimen to 'feed' a growing crack in elastic material. If large amounts of plastic deformation occur when a cracked specimen is loaded, much energy absorbed by the specimen is not recovered upon unloading or crack advance (Anderson, 2005). In such a situation, Eqn 19 relates *J* to the difference in energy absorbed by identical specimens with two different crack sizes.

Although derived for non-linear elastic behavior (Fig. 1B), *J* can be applied to the loading portion of an elastic–plastic stress–strain curve (e.g. Fig. 1C). The *J*-integral is not defined for unloading. Nevertheless, ΔJ has been successfully correlated with crack growth rate, da/dN, for repeated cycles of loading and unloading (Dowling and Begley, 1976) even when gross amounts of plasticity accompany crack growth. With such correlations, *J* can be used, as described for G and T, to predict lifetime of materials with cracks, including seaweeds.

Furthermore, for some elastomeric materials and certain specimen designs, energy dissipates during specimen deformation and does not contribute to cracking processes.
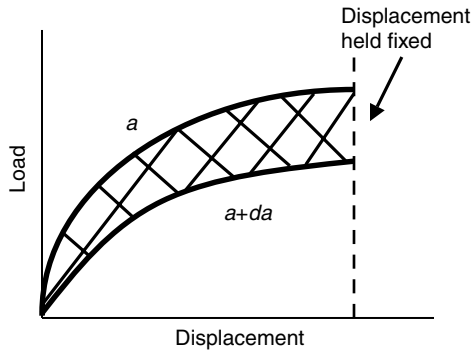
Fig. 11. Schematic showing change in load–displacement curves of specimens with two different crack lengths (*a* and *a+da*) but the same specimen displacement.

This dissipated energy should be separated from energy that contributes to cracking in determining fracture resistance. *J* may provide a means of partitioning energy in the crack-tip region from energy dissipated in the bulk of a specimen (Lee and Donovan, 1985).

Because it accommodates non-linear stress–strain curves and extensive plastic deformation at crack tips during loading, *J* may be another fracture parameter that could be fruitfully applied to macroalgal fracture processes.

Conclusions

Macroalgae frequently incur cracks due to herbivory, abrasion and fatigue. The fracture mechanics methods outlined here allow assessment of material strength reduction in the presence of cracks and of the effects of stresses below a material's ultimate strength. In repeated loadings imposed by breaking waves, cracks in macroalgal materials likely grow even when individual forces are not sufficient to cause complete fracture. These methods suggest a first avenue for investigating seaweed breakage in the realistic context of repeated wave force imposition.

Furthermore, the methods presented from LEFM, fracture mechanics of elastomers and elastic–plastic fracture mechanics enable prediction of the lifetime for breakage of other biological materials with cracks or flaws in the presence of isolated large loads or of repeated loadings. Although incremental crack growth at sub-critical loads has been largely ignored for many biological materials, such fatigue crack growth may contribute importantly to ecologically, evolutionarily and physiologically relevant breakage in organisms ranging from seaweeds to terrestrial plants to animals.

Appendix A

Critical strain energy release rate, T_C, may be found experimentally through the following procedure. Specimens with introduced cracks of different lengths *a* (m) are pulled until unstable tearing occurs. For the various tested specimens, load (N), applied to a specimen until it tears

completely, is plotted against specimen displacement δ (m), the difference between specimen length at a given time and initial specimen length (Fig. A1A).
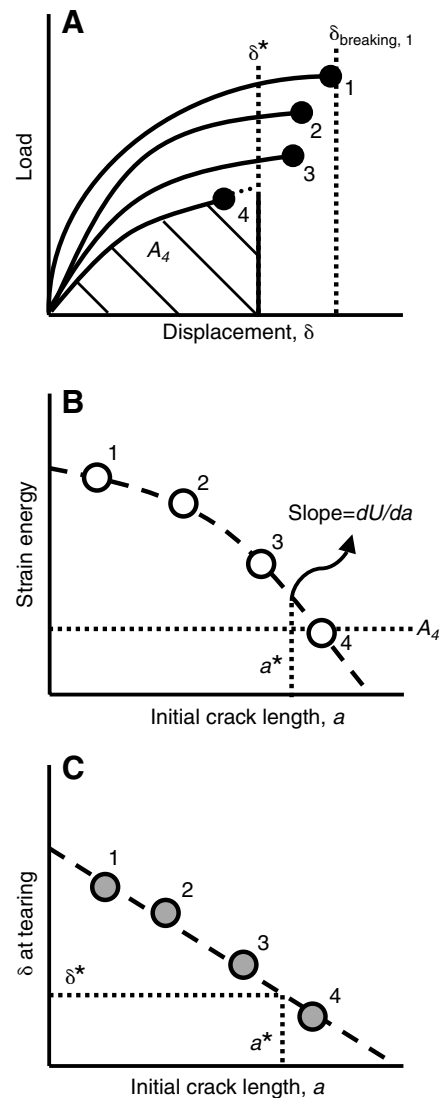

Fig. A1. Plots used in experimental determination of critical strain energy release rate. (A) Load–displacement plots for specimens with various initial crack lengths. Solid circles indicate points at which unstable tearing occurred. Lower curves are for specimens with longer initial cracks. δ* represents a displacement chosen for generation of plot (B). Area 4, A_4 (hatched), indicates strain energy present in specimen 4 when it is pulled to displacement δ*; specimen 4's load–displacement curve must be extrapolated. $δ_{breaking,1}$ indicates the displacement at which specimen 1 tore unstably, which is used for plot (C). (B) A plot, derived from (A), of strain energy *versus* initial crack length at a selected value of specimen displacement, δ*. For example, strain energy A_4 is plotted against the length of specimen 4's initial crack, as depicted by the open circle 4. (C) A plot, derived from (A), of displacement at tearing *versus* initial crack length. For example, $δ_{breaking,1}$ is plotted against specimen 1's initial crack length, as indicated by grey circle 1. From this plot, initial crack length, *a**, corresponding to δ*, is determined. At this value of *a**, the tangent to plot (B) is found, which gives (*dU/da*).

For a selected value of specimen displacement, δ^*, a plot of stored strain energy U (J) *versus* initial crack length is constructed (Fig. A1B). Given elastic material behavior, stored strain energy is the area under the load–displacement curve, in this case between zero displacement and δ^* (Fig. A1A). If unstable tearing occurs before a specimen reaches the selected displacement, the specimen's load–deformation curve in Fig. A1A is extrapolated to estimate stored energy.

Then, a third plot (Fig. A1C) of specimen displacement at tearing *versus* initial crack length is generated from the load–displacement plots in Fig. A1A. From this plot, for the displacement selected for Fig. A1B, δ^*, one determines initial crack length, a^*, for which tearing would have occurred at the given displacement from a line fitted to the data points. At this value of a^*, the tangent to the *U-versus-a* curve (Fig. A1B) is determined. This tangent (or slope) yields dU/da, which can be converted to critical strain energy release rate, T_C, or $-dU/dA$, by multiplying the tangent by -1/specimen thickness. Any selected value of specimen displacement for construction of the second plot (Fig. A1B) should yield approximately the same value of T_C.

Appendix B

The *J*-integral (Rice, 1968a; Rice, 1968b) is given by the line integral:

$$J = \int_\Gamma \left(W dy - \mathbf{P} \cdot \frac{\partial \mathbf{u}}{\partial x} \, ds \right), \tag{A1}$$

where Γ is a path-independent, counterclockwise contour surrounding a crack tip, W is strain energy density, and $\mathbf{P}$ is a stress vector acting on an element of path length ds (Fig. A2A). $\mathbf{P}$ is defined according to the outward-direction, unit-vector normal to Γ, $\mathbf{n}$ (Fig. A2A; see Eqn A2 and Eqn A3 below). In Fig. A2A, $\mathbf{u}$ denotes a vector quantifying displacement of the material at the same location (ds), while ($\partial \mathbf{u}/\partial x$) is a displacement gradient (see Eqn A4 and Eqn A5 below). Although the stress (traction) vector is usually notated with '$\mathbf{T}$', here we use '$\mathbf{P}$' to avoid confusion with strain energy release rate T.

To explain these terms and illustrate evaluation of the integral, two-dimensional stress will be considered. Two-dimensional stress occurs, for example, in a stretched thin sheet of material. It is described by three stress components, σ_x, σ_y, and τ_{xy}, acting on a small element of material (Fig. A2B). The σ_x and σ_y components elongate (or compress) material, while the τ_{xy} component shears material. Also for illustration, a rectangular contour Γ around a crack tip will be considered, depicted in Fig. A2C.

The traction vector $\mathbf{P}$ can be expressed as $P_x \mathbf{i} + P_y \mathbf{j}$, where $\mathbf{i}$ and $\mathbf{j}$ are unit vectors in the x and y directions, respectively. P_x and P_y can be found from:

$$P_x = n_x \sigma_x + n_y \tau_{xy} , \tag{A2}$$
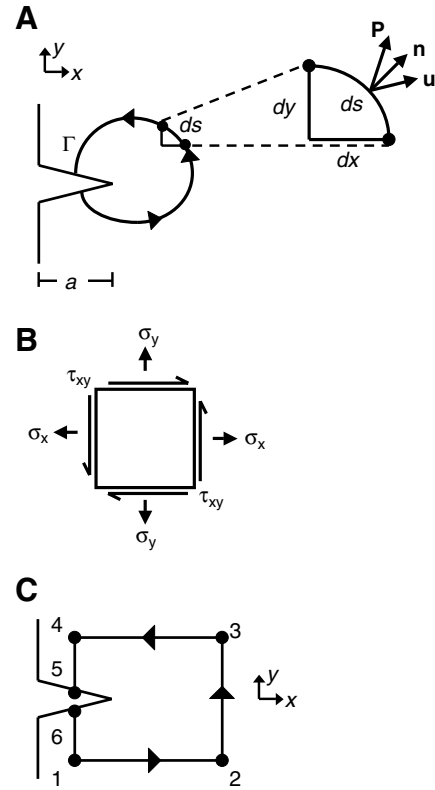
$$P_y = n_x \tau_{xy} + n_y \sigma_y , \tag{A3}$$

Fig. A2. (A) Counterclockwise contour Γ around a crack tip showing an element of path length ds, with unit vector $\mathbf{n}$ normal to the path and with stress and displacement vectors, $\mathbf{P}$ and $\mathbf{u}$, respectively, also shown. Crack length is a. (B) An element of material experiencing two-dimensional stress. Not all three stress components need be active; often only one or two components are active. (C) Rectangular path Γ surrounding a crack tip, used to illustrate evaluation of a *J*-integral.

where n_x and n_y are components of the outward unit vector $\mathbf{n}$ normal to a segment. For instance, along the segment 1–2 in Fig. A2C, $(n_x, n_y)=(0, -1)$, so that $P_x=-\tau_{xy}$ and $P_y=-\sigma_y$. Along 2–3, $(n_x, n_y)=(1, 0)$, so that $P_x=\sigma_x$ and $P_y=\tau_{xy}$. Along 3–4, $(n_x, n_y)=(0, 1)$ so that $P_x=\tau_{xy}$ and $P_y=\sigma_y$. Along 4–5 and 6–1, $(n_x, n_y)=(-1, 0)$, yielding $P_x=-\sigma_x$ and $P_y=-\tau_{xy}$.

Deformation of an object is commonly represented by a displacement vector that describes the change in coordinates of a point in the object, from (x_1, y_1) to (x_2, y_2). The vector is given by:

$$\mathbf{u} = u\mathbf{i} + v\mathbf{j} , \tag{A4}$$

where $u=x_2-x_1$ and $v=y_2-y_1$ (Boresi, 2000). The vector can vary in magnitude and direction from one location to another in an object. Differentiation of Eqn A4 leads to:

$$\frac{\partial \mathbf{u}}{\partial x} = \frac{\partial u}{\partial x} \mathbf{i} + \frac{\partial v}{\partial x} \mathbf{j} . \tag{A5}$$

Forming the scalar product $\mathbf{P} \cdot (\partial \mathbf{u}/\partial x)$ along segment 1–2 yields

$$-\tau_{xy} \frac{\partial u}{\partial x} - \sigma_y \frac{\partial v}{\partial x} ;$$

along segment 3–4, the product is the same, except multiplied by –1 throughout. Along segment 2–3, the product is

$$\sigma_x \frac{\partial u}{\partial x} + \tau_{xy} \frac{\partial v}{\partial x} \, ;$$

along segments 4–5 and 6–1, the product is the same, except again multiplied by –1 throughout.

Each segment will contribute to the *J*-integral as indicated in Table A1. Note that along this rectilinear path *ds* becomes either *dx* or *dy*, depending on the segment.

The strain energy density term along a segment can be evaluated for two-dimensional stress from

$$W = \int (\sigma_x d\epsilon_x + \sigma_y d\epsilon_y + \tau_{xy} d\gamma_{xy}) \,, \qquad (A6)$$

where ϵ_x, ϵ_y, and γ_{xy} are normal (ϵ) and shear (γ) strain components present along a segment. Integration is carried out from the initial state (no strains) to the final state (maximum strains reached).

Several approaches exist for evaluating the terms in the *J*-integral when significant plastic straining is present. For example, the displacement terms $\partial u/\partial x$ and $\partial v/\partial x$, as well as $\partial u/\partial y$ and $\partial v/\partial y$, can be found by optical methods such as Moire interferometry (Dadkhah and Kobayashi, 1990), digital image correlation (Sutton et al., 1991), and electronic speckle pattern interferometry (Moore and Tyrer, 1994). Corresponding strains can then be computed from $\epsilon_x=\partial u/\partial x$, $\epsilon_y=\partial v/\partial y$ and $\gamma_{xy}=\frac{1}{2}[(\partial u/\partial y)+(\partial v/\partial x)]$. From a material's stress–strain curve, stress components σ_x, σ_y and τ_{xy} can be computed from these strain components using relations between stresses and strains available from the theory of plasticity (Sutton et al., 1996; Chakrabarty, 2006). If a contour is taken far enough from a crack-tip region to make plastic straining negligible, simpler linear elastic stress–strain relations can then be used (Kawahara and Brandon, 1983). Determination of the variation of displacements, strains and stresses along the segments of the contour provides input to the evaluation of the terms in the line integrals in Table A1. The variation of a given term (e.g. *W*) along a segment can be fitted by a mathematical function of *x* or *y* to facilitate integration (Read, 1983).

Table A1. *Contributions to J-integral for rectangular path*

Segments	Contribution along each segment
1–2 and 3–4 (*dy*=0)	$\int \left(\tau_{xy} \dfrac{\partial u}{\partial x} + \sigma_y \dfrac{\partial v}{\partial x} \right) dx$
2–3, 4–5 and 6–1 (*dx*=0)	$\int \left[W - \left(\sigma_x \dfrac{\partial u}{\partial x} + \tau_{xy} \dfrac{\partial v}{\partial x} \right) \right] dy$

The *J*-integral may also be determined using commercially available finite element programs that compute the terms involved in the integral from loads applied to a given specimen geometry, without the need for experimental data other than a stress–strain curve.

List of symbols and abbreviations

Equation in which each symbol is first used is given (if symbol is used in an equation).

A	crack surface area, Eqn 4
a	measure of crack length, Eqn 1
a_1	initial crack length, Eqn 17
a_2	final crack length, Eqn 17
B	fitted constant, Eqn 16
b	thickness, Eqn 11
C	cross-sectional area of trouser-tear test piece, Eqn 11
c	leg width of trouser-tear test piece
d	crack-tip diameter, Eqn 8
ds	contour element path length, Eqn A1
da/dN	crack growth rate, Eqn 15
E	modulus of elasticity, Eqn 5
f(a/w)	dimensionless function of the crack geometry and sheet width , Eqn 1
F	force, Eqn 11
G	strain energy release rate, Eqn 4
G_C	critical strain energy release rate, Eqn 7
G_I	strain energy release rate (mode I loading), Eqn 5
J	*J*-integral, Eqn 19
J_C	critical value of *J*
J_I	*J* for mode I loading
K_C	critical stress intensity factor, fracture toughness, Eqn 3
K_I	stress intensity factor (mode I loading), Eqn 1
k	specimen extension parameter, Eqn 9
LEFM	linear elastic fracture mechanics
N	cycle number, Eqn 17
n	normal vector
P	traction vector, Eqn A1
R	crack resistance
t	thickness
T	strain energy release rate, Eqn 8
T_C	critical strain energy release rate, Eqn 11
T_I	strain energy release rate (mode I loading), Eqn 9
U	strain energy, Eqn 4
u	displacement vector, Eqn A1
V	energy absorbed during crack extension
W	strain energy density in crack-tip region, Eqn 8
W_o	strain energy density in bulk of specimen, Eqn 9
w	width, Eqn 1
β	fitted constant, Eqn 16
Γ	contour surrounding crack tip, Eqn A1
Δ*J*	range of *J*-integral
ΔK_I	range of stress intensity factor (mode I loading)

ΔK_{TH}	threshold range of stress intensity factor
ΔT	range of strain energy release rate
$\Delta\sigma$	range of applied stress
δ	displacement
λ_{max}	maximum extension ratio
ϵ	normal strain component, Eqn A6
τ_{xy}	shear stress component, Eqn A2
γ	shear strain component, Eqn A6
σ	applied stress, Eqn 1
σ_C	strength of specimen with crack, Eqn 3
θ	crack-tip angle, Eqn 8
λ	extension ratio, Eqn 10
Λ	energy released in crack extension (trouser-tear test), Eqn 13

References

Ahagon, A., Gent, A. N., Kim, H. J. and Kumagai, Y. (1975). Fracture energy of elastomers in mode I (cleavage) and mode III (lateral shear). *Rubber Chem. Technol.* **48**, 896-901.

Anderson, T. L. (2005). *Fracture Mechanics: Fundamentals and Applications* (3rd edn). Boca Raton: CRC Press.

Andrews, E. H. (1968). *Fracture in Polymers.* New York: American Elsevier.

Armstrong, S. L. (1987). Mechanical properties of the tissues of the brown alga *Hedophyllum sessile* (C. Ag.) Setchell: variability with habitat. *J. Exp. Mar. Biol. Ecol.* **114**, 143-151.

Atkins, A. G. and Mai, Y.-W. (1985). *Elastic and Plastic Fracture: Metals, Polymers, Ceramics, Composites, Biological Materials.* New York: Halsted Press.

Behiri, J. C. and Bonfield, W. (1984). Fracture mechanics of bone – the effects of density, specimen thickness and crack velocity on longitudinal fracture. *J. Biomech.* **17**, 25-34.

Bertness, M. D. and Leonard, G. H. (1997). The role of positive interactions in communities: lessons from intertidal habitats. *Ecology* **78**, 1976-1989.

Bertram, J. E. A. and Gosline, J. M. (1986). Fracture toughness design in horse hoof keratin. *J. Exp. Biol.* **125**, 29-47.

Biedka, R. F., Gosline, J. M. and DeWreede, R. E. (1987). Biomechanical analysis of wave-induced mortality in the marine alga *Pterygophora californica. Mar. Ecol. Prog. Ser.* **36**, 163-170.

Black, R. (1976). The effects of grazing by the limpet, *Acmaea insessa*, on the kelp, *Egregia laevigata*, in the intertidal zone. *Ecology* **57**, 265-277.

Blanchette, C. A. (1997). Size and survival of intertidal plants in response to wave action: a case study with *Fucus gardneri. Ecology* **78**, 1563-1578.

Boller, M. L. and Carrington, E. (2006a). *In situ* measurements of hydrodynamic forces imposed on *Chondrus crispus* Stackhouse. *J. Exp. Mar. Biol. Ecol.* **337**, 159-170.

Boller, M. L. and Carrington, E. (2006b). The hydrodynamic effects of shape and size change during reconfiguration of a flexible macroalga. *J. Exp. Biol.* **209**, 1894-1903.

Boresi, A. P. (2000). *Elasticity in Engineering Mechanics* (2nd edn). New York: Wiley.

Bose, W. W. and Landes, J. D. (2003). Fracture toughness of thin polymer films using miniature specimens. *J. Test. Eval.* **31**, 304-310.

Boulding, E. G. and LaBarbera, M. (1986). Fatigue damage: repeated loading enables crabs to open larger bivalves. *Biol. Bull.* **171**, 538-547.

Broek, D. (1982). *Elementary Engineering Fracture Mechanics.* Boston: Martinus Nijhoff Publishers.

Broek, D. (1989). *The Practical Use of Fracture Mechanics.* Boston: Kluwer Academic Publishers.

Busfield, J. J. C., Jha, V., Liang, H., Papadopoulos, I. C. and Thomas, A. G. (2005). Prediction of fatigue crack growth using finite element analysis techniques applied to three-dimensional elastomeric components. *Plast. Rubber Compos.* **34**, 349-356.

Caler, W. E. and Carter, D. R. (1989). Bone creep-fatigue damage accumulation. *J. Biomech.* **22**, 625-635.

Carrington, E. (1990). Drag and dislodgment of an intertidal macroalga: consequences of morphological variation in *Mastocarpus papillatus* Kützing. *J. Exp. Mar. Biol. Ecol.* **139**, 185-200.

Carrington, E., Grace, S. P. and Chopin, T. (2001). Life history phases and the biomechanical properties of the red alga *Chondrus crispus* (Rhodophyta). *J. Phycol.* **37**, 699-704.

Chakrabarty, J. (2006). *Theory of Plasticity* (3rd edn). Amsterdam: Elsevier.

Connell, J. H. (1978). Diversity in tropical rain forests and coral reefs. *Science* **199**, 1302-1310.

Currey, J. D. (1998). Mechanical properties of vertebrate hard tissues. *Proc. Inst. Mech. Eng.* **212**, 399-411.

Dadkhah, M. S. and Kobayashi, A. S. (1990). Further studies on the hrr field of a moving crack, an experimental analysis. *Int. J. Plast.* **6**, 635-650.

Davison, I. R. and Pearson, G. A. (1996). Stress tolerance in intertidal seaweeds. *J. Phycol.* **32**, 197-211.

Dayton, P. K. (1971). Competition, disturbance, and community organization: the provision and subsequent utilization of space in a rocky intertidal community. *Ecol. Monogr.* **41**, 351-389.

Denny, M. W. (1988). *Biology and the Mechanics of the Wave-Swept Environment.* Princeton: Princeton, University Press.

Denny, M. W. (2006). Ocean waves, nearshore ecology, and natural selection. *Aquatic Ecol.* **40**, 439-461.

Denny, M. and Gaylord, B. (2002). The mechanics of wave-swept algae. *J. Exp. Biol.* **205**, 1355-1362.

Denny, M. and Wethey, D. (2001). Physical processes that generate patterns in marine communities. In *Marine Community Ecology* (ed. M. D. Bertness, S. D. Gaines and M. E. Hay), pp. 3-37. Sunderland: Sinauer Associates.

Denny, M., Brown, V., Carrington, E., Kraemer, G. and Miller, A. (1989). Fracture mechanics and the survival of wave-swept macroalgae. *J. Exp. Mar. Biol. Ecol.* **127**, 211-228.

Denny, M. W., Gaylord, B. P. and Cowen, E. A. (1997). Flow and flexibility. II. The roles of size and shape in determining wave forces on the bull kelp *Nereocystis luetkeana. J. Exp. Biol.* **200**, 3165-3183.

Denny, M. W., Miller, L. P., Stokes, M. D., Hunt, L. J. H. and Helmuth, B. S. T. (2003). Extreme water velocities: topographical amplification of wave-induced flow in the surf zone of rocky shores. *Limnol. Oceanogr.* **48**, 1-8.

DeWreede, R. E., Ewanchuk, P. and Shaughnessy, F. (1992). Wounding, healing and survivorship in three kelp species. *Mar. Ecol. Prog. Ser.* **82**, 259-266.

Dorfmann, A. and Ogden, R. W. (2004). A constitutive model for the Mullins effect with permanent set in particle-reinforced rubber. *Int. J. Solids Struct.* **41**, 1855-1878.

Dorfmann, A., Trimmer, B. A. and Woods, W. A. (2007). A constitutive model for muscle properties in a soft-bodied arthropod. *J. R. Soc. Interface* **4**, 257-269.

Dowling, N. E. and Begley, J. A. (1976). Fatigue crack growth during gross plasticity and the J-integral. In *Mechanics of Crack Growth, ASTM STP 590*, pp. 82-103. Philadelphia: American Society for Testing and Materials.

Dudgeon, S. R. and Johnson, A. S. (1992). Thick vs. thin: thallus morphology and tissue mechanics influence differential drag and dislodgment of two co-dominant seaweeds. *J. Exp. Mar. Biol. Ecol.* **165**, 23-43.

Dudgeon, S. R., Steneck, R. S., Davison, I. R. and Vadas, R. L. (1999). Coexistence of similar species in a space-limited intertidal zone. *Ecol. Monogr.* **69**, 331-352.

Farquhar, T. and Zhao, Y. (2006). Fracture mechanics and its relevance to botanical structures. *Am. J. Bot.* **93**, 1449-1454.

Friedland, M. T. and Denny, M. W. (1995). Surviving hydrodynamic forces in a wave-swept environment: Consequences of morphology in the feather boa kelp, *Egregia menziesii* (Turner). *J. Exp. Mar. Biol. Ecol.* **190**, 109-133.

Gaylord, B. (1999). Detailing agents of physical disturbance: wave-induced velocities and accelerations on a rocky shore. *J. Exp. Mar. Biol. Ecol.* **239**, 85-124.

Gaylord, B. (2000). Biological implications of surf-zone flow complexity. *Limnol. Oceanogr.* **45**, 174-188.

Gaylord, B. and Denny, M. W. (1997). Flow and flexibility. I. Effects of size, shape and stiffness in determining wave forces on the stipitate kelps *Eisenia arborea* and *Pterygophora californica*. *J. Exp. Biol.* **200**, 3141-3164.

Gaylord, B., Blanchette, C. A. and Denny, M. W. (1994). Mechanical consequences of size in wave-swept algae. *Ecol. Monogr.* **64**, 287-313.

Gosline, J., Lillie, M., Carrington, E., Guerette, P., Ortlepp, C. and Savage, K. (2002). Elastic proteins: biological roles and mechanical properties. *Philos. Trans. R. Soc. Lond. B Biol. Sci.* **357**, 121-132.

Greensmith, H. W. (1963). Rupture of rubber. X. The change in stored energy on making a small cut in a test piece held in simple extension. *J. Appl. Polym. Sci.* **7**, 993-1002.

Greensmith, H. W. and Thomas, A. G. (1955). Rupture of rubber. III. Determination of tear properties. *J. Polym. Sci.* **18**, 189-200.

Hale, B. (2001). Macroalgal materials: foiling fracture and fatigue from fluid forces. PhD thesis, Stanford University, USA.

Harley, C. D. G. and Helmuth, B. S. T. (2003). Local- and regional-scale effects of wave exposure, thermal stress, and absolute versus effective shore level on patterns of intertidal zonation. *Limnol. Oceanogr.* **48**, 1498-1508.

Hawes, I. and Smith, R. (1995). Effect of current velocity on the detachment of thalli of *Ulva lactuca* (Chlorophyta) in a New Zealand estuary. *J. Phycol.* **31**, 875-880.

Helmuth, B. and Denny, M. W. (2003). Predicting wave exposure in the rocky intertidal zone: do bigger waves always lead to larger forces? *Limnol. Oceanogr.* **48**, 1338-1345.

Hofmann, G. E. and Somero, G. N. (1995). Evidence for protein damage at environmental temperatures: seasonal changes in levels of ubiquitin conjugates and hsp70 in the intertidal mussel *Mytilus trossulus*. *J. Exp. Biol.* **198**, 1509-1518.

Holbrook, N. M., Denny, M. W. and Koehl, M. A. R. (1991). Intertidal 'trees': consequences of aggregation on the mechanical and photosynthetic properties of sea-palms *Postelsia palmaeformis* Ruprecht. *J. Exp. Mar. Biol. Ecol.* **146**, 39-67.

Joe, C. R. and Kim, B. H. (1990). A method to determine the *R*-curve of flexible materials using a monotonic loading of a single trouser tear specimen. *Int. J. Fract.* **44**, 15-26.

Johnson, A. S. (2001). Drag, drafting, and mechanical interactions in canopies of the red alga *Chondrus crispus*. *Biol. Bull.* **201**, 126-135.

Johnson, A. S. and Koehl, M. A. R. (1994). Maintenance of dynamic strain similarity and environmental stress factor in different flow habitats: thallus allometry and material properties of a giant kelp. *J. Exp. Biol.* **195**, 381-410.

Johnson, C. R. and Mann, K. H. (1986). The importance of plant defence abilities to the structure of subtidal seaweed communities: the kelp *Laminaria longicruris* de la Pylaie survives grazing by the snail *Lacuna vincta* (Montagu) at high population densities. *J. Exp. Biol. Mar. Ecol.* **97**, 231-267.

Kanninen, M. F. and Popelar, C. H. (1985). *Advanced Fracture Mechanics.* New York: Oxford University Press.

Kasapi, M. A. and Gosline, J. M. (1996). Strain-rate-dependent mechanical properties of the equine hoof wall. *J. Exp. Biol.* **199**, 1133-1146.

Kasapi, M. A. and Gosline, J. M. (1997). Design complexity and fracture control in the equine hoof wall. *J. Exp. Biol.* **200**, 1639-1659.

Kawahara, W. A. and Brandon, S. L. (1983). *J*-integral evaluation by resistance strain gauges. *Eng. Fract. Mech.* **18**, 427-434.

Keaveny, T. M., Morgan, E. F., Niebur, G. L. and Yeh, O. C. (2001). Biomechanics of trabecular bone. *Annu. Rev. Biomed. Eng.* **3**, 307-333.

Kim, B. H., Joe, C. R. and Otterson, D. M. (1989). On the determination of fracture toughness in polymers. *Polym. Test.* **8**, 119-130.

Kitzes, J. A. and Denny, M. W. (2005). Red algae respond to waves: morphological and mechanical variation in *Mastocarpus papillatus* along a gradient of force. *Biol. Bull.* **208**, 114-119.

Koehl, M. A. R. (1984). How do benthic organisms withstand moving water? *Am. Zool.* **24**, 57-70.

Koehl, M. A. R. (1986). Seaweeds in moving water: form and mechanical function. In *On the Economy of Plant Form and Function* (ed. T. J. Givnish), pp. 603-634. Cambridge: Cambridge University Press.

Koehl, M. A. R. and Alberte, R. S. (1988). Flow, flapping, and photosynthesis of *Nereocystis luetkeana*: a functional comparison of undulate and flat blade morphologies. *Mar. Biol.* **99**, 435-444.

Koehl, M. A. R. and Wainwright, S. A. (1977). Mechanical adaptations of a giant kelp. *Limnol. Oceanogr.* **22**, 1067-1071.

Kuhn-Spearing, L. T., Kessler, H., Chateau, E., Ballarini, R., Heuer, A. H.

and Spearing, S. M. (1996). Fracture mechanisms of the *Strombus gigas* conch shell: implications for the design of brittle laminates. *J. Mater. Sci.* **31**, 6583-6594.

LaBarbera, M. and Merz, R. A. (1992). Postmortem changes in strength of gastropod shells: evolutionary implications for hermit crabs, snails, and their mutual predators. *Paleobiology* **18**, 367-377.

Lake, G. J. (1983). Aspects of fatigue and fracture of rubber. *Prog. Rubber Technol.* **45**, 89-143.

Lake, G. J. (1995). Fatigue and fracture of elastomers. *Rubber Chem. Technol.* **68**, 435-460.

Lee, D. J. and Donovan, J. A. (1985). Critical *J*-integral and tearing energies for fracture of reinforced natural rubber. *Theor. Appl. Fract. Mech.* **4**, 137-147.

Leigh, E. G., Paine, R. T., Quinn, J. F. and Suchanek, T. H. (1987). Wave energy and intertidal productivity. *Proc. Natl. Acad. Sci. USA* **84**, 1314-1318.

Lindley, P. B. (1972). Energy for crack growth in model rubber components. *J. Strain Anal.* **7**, 132-140.

Lowell, R. B., Markham, J. H. and Mann, K. H. (1991). Herbivore-like damage induces increased strength and toughness in a seaweed. *Proc. R. Soc. Lond. B Biol. Sci.* **243**, 31-38.

Mach, K. J., Hale, B. B., Denny, M. W. and Nelson, D. V. (2007). Death by small forces: a fracture and fatigue analysis of wave-swept macroalgae. *J. Exp. Biol.* **210**, 2231-2243.

Mai, Y. W. and Cotterell, B. (1984). The essential work of fracture for tearing of ductile metals. *Int. J. Fract.* **24**, 229-236.

Mars, W. V. and Fatemi, A. (2003). Fatigue crack nucleation and growth in filled natural rubber. *Fatigue Fract. Eng. Mater. Struct.* **26**, 779-789.

Martone, P. T. (2006). Size, strength and allometry of joints in the articulated coralline *Calliarthron*. *J. Exp. Biol.* **209**, 1678-1689.

Menge, B. A. (1995). Indirect effects in marine rocky intertidal interaction webs: patterns and importance. *Ecol. Monogr.* **65**, 21-74.

Moore, A. J. and Tyrer, J. R. (1994). Evaluation of fracture mechanics' parameters using electronic speckle pattern interferometry. *J. Strain Anal.* **29**, 257-262.

Nelson, D. V. (1977). Review of fatigue-crack-growth prediction methods. *Exp. Mech.* **17**, 41-49.

Oh, H. L. (1976). A simple method for measuring tearing energy of nicked rubber strips. In *Mechanics of Crack Growth*, *ASTM STP 590*, pp. 104-114. Philadelphia: American Society for Testing and Materials.

Paine, R. T. (1966). Food web complexity and species diversity. *Am. Nat.* **100**, 65-75.

Paine, R. T. (1984). Ecological determinism in the competition for space: the Robert H. MacArthur award lecture. *Ecology* **65**, 1339-1348.

Perez, N. (2004). *Fracture Mechanics*. Boston: Kluwer Academic Publishers.

Pook, L. P. (1983). *The Role of Crack Growth in Metal Fatigue*. London: The Metals Society.

Pratt, M. C. and Johnson, A. S. (2002). Strength, drag, and dislodgment of two competing intertidal algae from two wave exposures and four seasons. *J. Exp. Mar. Biol. Ecol.* **272**, 71-101.

Purslow, P. P. (1983). Measurement of the fracture toughness of extensible connective tissues. *J. Mater. Sci.* **18**, 3591-3598.

Purslow, P. P. (1989). Fracture of non-linear biological materials: some observations from practice relevant to theory. *J. Phys. D Appl. Phys.* **22**, 854-856.

Read, D. T. (1983). Experimental method for direct evaluation of the *J*-contour integral. In *Fracture Mechanics, Fourteenth Symposium, Volume II: Testing and Applications*, *ASTM STP 791*, pp. 199-213. Philadelphia: American Society for Testing and Materials.

Rice, J. R. (1968a). A path independent integral and the approximate analysis of strain concentration by notches and cracks. *J. Appl. Mech.* **35**, 379-386.

Rice, J. R. (1968b). Mathematical analysis in the mechanics of fracture. In *Fracture, An Advanced Treatise*. Vol. 2 (ed. H. Liebowitz), pp. 191-311. New York: Academic Press.

Rivlin, R. S. and Thomas, A. G. (1953). Rupture of rubber. I. Characteristic energy for tearing. *J. Polym. Sci.* **10**, 291-318.

Sanford, R. J. (2003). *Principles of Fracture Mechanics.* Upper Saddle River, NJ: Prentice Hall.

Saxena, A. (1998). *Nonlinear Fracture Mechanics for Engineers.* Boston: CRC Press.

Schubel, P. M., Gdoutos, E. E. and Daniel, I. M. (2004). Fatigue characterization of tire rubber. *Theor. Appl. Fract. Mech.* **42**, 149-154.

Seldén, R. (1995). Fracture mechanics analysis of fatigue of rubber – a review. *Prog. Ser. Rubber Plast. Technol.* **11**, 56-83.

Seymour, R. J., Tegner, M. J., Dayton, P. K. and Parnell, P. E. (1989). Storm wave induced mortality of giant kelp, *Macrocystis pyrifera*, in Southern California. *Estuar. Coast. Shelf Sci.* **28**, 277-292.

Shaughnessy, F. J., DeWreede, R. E. and Bell, E. C. (1996). Consequences of morphology and tissue strength to blade survivorship of two closely related Rhodophyta species. *Mar. Ecol. Prog. Ser.* **136**, 257-266.

Shigley, J. E. and Mischke, C. R. (2001). *Mechanical Engineering Design* (6th edn). San Francisco: McGraw-Hill.

Smith, S. V. and Kinsey, D. W. (1976). Calcium carbonate production, coral reef growth, and sea level change. *Science* **194**, 937-939.

Somero, G. N. (2002). Thermal physiology and vertical zonation of intertidal animals: optima, limits, and costs of living. *Int. Comp. Biol.* **42**, 780-789.

Spatz, H.-Ch., Köhler, L. and Niklas, K. J. (1999). Mechanical behaviour of plant tissues: composite materials or structures? *J. Exp. Biol.* **202**, 3269-3272.

Stillman, J. H. (2002). Causes and consequences of thermal tolerance limits in rocky intertidal porcelain crabs, genus *Petrolisthes*. *Int. Comp. Biol.* **42**, 790-796.

Stillman, J. H. and Somero, G. N. (1996). Adaptation to temperature stress and aerial exposure in congeneric species of intertidal porcelain crabs (genus *Petrolisthes*): correlation of physiology, biochemistry and morphology with vertical distribution. *J. Exp. Biol.* **199**, 1845-1855.

Sutton, M. A., Turner, J. L., Bruck, H. A. and Chae, T. A. (1991). Full-field representation of discretely sampled surface deformation for displacement and strain analysis. *Exp. Mech.* **31**, 168-177.

Sutton, M. A., Deng, X., Liu, J. and Yang, L. (1996). Determination of elastic-plastic stresses and strains from measured surface strain data. *Exp. Mech.* **36**, 99-112.

Taylor, D. and Lee, T. C. (2003). A crack growth model for the simulation of fatigue in bone. *Int. J. Fatigue* **25**, 387-395.

Thomas, A. G. (1955). Rupture of rubber. II. The strain concentration at an incision. *J. Polym. Sci.* **18**, 177-188.

Thomas, A. G. (1994). The development of fracture mechanics for elastomers. *Rubber Chem. Technol.* **67**, G50-G60.

Tomanek, L. (2002). The heat-shock response: its variation, regulation and ecological importance in intertidal gastropods (genus *Tegula*). *Int. Comp. Biol.* **42**, 797-807.

Tomanek, L. and Helmuth, B. (2002). Physiological ecology of rocky intertidal organisms: a synergy of concepts. *Int. Comp. Biol.* **42**, 771-775.

Utter, B. D. and Denny, M. W. (1996). Wave-induced forces on the giant kelp *Macrocystis pyrifera* (Agardh): field test of a computational model. *J. Exp. Biol.* **199**, 2645-2654.

Wainstein, J., Frontini, P. M. and Cassanelli, A. N. (2004). *J-R* curve determination using the load separation parameter S_{pb} method for ductile polymers. *Polym. Test.* **23**, 591-598.

Vincent, J. F. V. (1991). Strength and fracture of grasses. *J. Mater. Sci.* **26**, 1947-1950.

Vogel, S. (1984). Drag and flexibility in sessile organisms. *Am. Zool.* **24**, 37-44.

Wolcott, T. G. (1973). Physiological ecology and intertidal zonation in limpets (*Acmaea*): a critical look at 'limiting factors'. *Biol. Bull.* **145**, 389-422.

Yeoh, O. H. (2002). Relation between crack surface displacements and strain energy release rate in thin rubber sheets. *Mech. Mater.* **34**, 459-474.